Surface Science 268 (1992) 418–431
North-Holland

surface science

Phonons on fcc (100), (110), and (111) surfaces using Lennard-Jones potentials

II. Temperature dependence of surface phonons studied with molecular dynamics

D.D. Koleske and S.J. Sibener

The Department of Chemistry and The James Franck Institute, The University of Chicago, 5640 South Ellis Avenue, Chicago, IL 60637, USA

Received 20 September 1991; accepted for publication 18 November 1991

In this paper we present temperature dependent studies of the surface phonon dispersion relations for fcc (100), (110), and (111) faces using molecular dynamics (MD) simulations and Lennard-Jones potentials. This study was conducted in order to investigate how anharmonic potential terms influence the dynamical properties of the surface. This was accomplished by examining the temperature dependence of the Q-resolved phonon spectral density function. All phonon frequencies were found to decrease linearly in T as the temperature was increased, while at low temperatures the phonon linewidths increased linearly with T. At higher temperatures, some of the phonon linewidths changed from having a linear to a quadratic dependence on T. The temperature at which this T to T^2 change occurs is surface dependent and occurs at the lowest temperature on the (110) surface. The T^2 dependence arises from the increasing importance of higher-order phonon–phonon scattering terms. The phonons which exhibit T^2 dependence tend to be modes which propagate perpendicularly or nearly perpendicularly to the direction of maximum root-mean-squared displacement (RMSD). This is especially true for the linewidth of the S_1 mode at $\bar{X}$ on the (110) surface where, at $T \approx 15$–23% of the melting temperature, the RMSD perpendicular to the atomic rows become larger than the RMSD normal to the surface. Our results indicate that the dynamics on the (110) surface may be significantly influenced by anharmonic potential terms at temperatures as low as 15% of the melting temperature.

1. Introduction

Many recent studies on the (110) faces of fcc metals have focussed on the changes in surface structure that occur as the surface is heated, specifically how the surface roughens and melts [1–9]. Most of these experimental and theoretical studies have concentrated on the static structural changes that occur at high temperatures, for example, the proliferation of steps as the roughening transition proceeds [1–4]. With the advent of surface vibrational spectroscopies such as high-resolution electron energy loss spectroscopy (HREELS) and helium atom scattering (HAS), several studies have been conducted on the thermal dependence of surface vibrations [9–13]. Mechanistically, these studies indicate that temperature-induced structural changes at the surface cannot be considered independently from temperature-induced anharmonic changes that occur in the surface vibrational properties [9–13].

An example of this are the two alternate interpretations that have been proposed to explain the high temperature behavior of the (110) surfaces of Ni and Cu, one interpretation being based on a structural change, and the other being based on a dynamical change in the surface vibrations. These two alternate interpretations have been proposed to explain the dramatic increase in the mean-square displacements (MSD) that have been observed on Cu(110) near $T = 870$ K. Previous X-ray studies have measured the decrease in specularly reflected signal, which was interpreted as an increase in the MSD normal to the surface [2]. The stronger than normal Debye–Waller increase in surface normal MSD was in turn attributed to an increase in the step density at the surface. However, the possible role that anhar-

monic potential terms play at elevated temperatures could not be ruled out [2]. Similar changes in MSD on Ni(110) were also observed in a high-Q-resolution low-energy electron diffraction (LEED) study at about half the melting temperature, T_m, of Ni [8]. In this study the authors concluded that the MSD parallel to the surface were 5 times larger than the MSD normal to the surface.

A similar drop in elastically scattered signal was also observed in HAS experiments on Cu(110) [9]. As the surface was heated up to ca. 700 K the reflected He signal dropped "rapidly" with increasing temperature [9]. However, HAS measurements of the diffuse elastic intensities on Cu(110) did not show an increase in the number of steps or defects up to $T = 900$ K [9]. The HAS results clearly indicate that no roughening occurs up to 900 K, and that the gradual drop in the intensity of the specularly reflected beam is most likely attributed to increased anharmonicity for this surface [9]. Also, no increase in the step density or adatom–vacancy pair defects were observed in MD simulations using effective-medium-theory (EMT) based potentials up to $T = 1000$ K [14]. Not until $T > 1000$ K are adatom–vacancy defect pairs observed on the simulated Cu(110) surface [14], with similar results being found at 1400 K for Ni(110) [15]. These studies clearly indicate that the initial increase in the MSD occurs because the surface atoms begin to significantly sample regions of the anharmonic potential at elevated temperatures.

The capability now exists to measure the phonon linewidth changes as a function of increasing temperature using HAS and HREELS. One recent example is the measurements of Baddorf and Plummer, who have directly monitored the increase in surface anharmonicity on Cu(110) by monitoring the phonon frequency decrease and linewidth dependence at $\bar{\Gamma}$ and $\bar{Y}$ [10,11]. From these measurements it was determined that the anharmonic influence at the surface is 4.1–4.8 times greater than in the bulk [10,11]. In another study, the one-phonon and multiphonon contributions to inelastic HAS intensities were calculated as a function of temperature on Cu(110) [16] and Cu(001) [17]. In both of these studies [16,17] the MSD were found to be influenced by phonon–phonon scattering terms proportional to temperature, but at temperatures near 600 K higher-order phonon–phonon interactions become significant, which have a quadratic temperature dependence. A larger anharmonic effect was found for the Cu(110) surface than for Cu(001) [16,17]. However, up to 600 K, the width of the S_3 mode $\bar{Y}$ on Cu(110) increased only linearly with temperature [10,11] and not quadratically.

In order to study and further quantify the influence that the anharmonic potential terms have on surface dynamics, we have performed molecular dynamics (MD) simulations using Lennard-Jones (LJ) potentials for fcc (100), (110), and (111) surfaces. These studies are similar in nature to our earlier studies on LJ(511) and LJ(533) stepped surfaces [18]. These earlier studies on stepped surfaces followed the energy width increase of the "edge modes" (E_1 and E_2 [19]) and Rayleigh wave (S_1) as a function of increasing temperature. In this earlier study the edge modes, which are localized on the step atoms, showed a greater increase in width than those of the terrace [18]. This indicates that a correlation exists between increased anharmonic effects and reduced coordination. From this we concluded that at elevated temperatures the increased importance of anharmonicity will influence phenomena ranging from surface melting and roughening to chemical transformations of the surface.

In a preceding paper referred to as paper I we outlined the method used to calculate the surface phonon spectral densities using MD simulations and compared these low-temperature results to calculations using the slab technique [20]. In this paper we focus on the dynamical changes which occur in the surface phonon spectral densities (i.e., frequency and linewidth changes) and root-mean-square displacements (RMSD) as a function of increasing temperature. Several authors have reported that at about $\frac{1}{2}T_m$ the (110) surface begins to disorder through the creation of adatom–vacancy pair defects. We will show how this disordering mechanism modifies the RMSD, and that adatom–vacancy pair creation reduces stress at the surface. We also compare the trends

seen in our results for LJ solids to the effective-medium theory (EMT) simulations [14] and HREELS measurements for Cu(110) [10,11].

2. Molecular dynamics method

Previous MD studies using LJ potentials have concentrated on the thermally induced changes in surface structure that occur as the surface is heated [21–25]. The temperature dependence of the surface vibrational properties averaged over all Q-vectors was previously studied [21,26], and in another study the Q-resolved phonon modes were calculated for the (100) surface at $\bar{X}$ for two temperatures [27]. Of the two temperatures reported, the S_4 (Rayleigh wave) mode at 53% T_m was noticeably wider than at 38% T_m [27]. This paper presents a much more extensive survey of how temperature influences the surface dynamical behavour of the (100), (110), and (111) surfaces. Our work also differs from previous work both in the total number of atoms simulated (3100 total) and the number of simulations (up to 40) performed to obtain the surface phonon spectral densities.

For each of the MD simulations the size of the parallelpiped slab ($l_x \times l_y \times l_z$) was $10 \times 10 \times 31$. A total of 3100 atoms were simulated with 100 atoms residing on each surface. The surface geometries, reciprocal lattices and major directions are shown in fig. 1. The lattice constant was assigned at the start of the simulation taking into account the thermal expansion of the lattice as previously discussed in paper I. All temperatures reported in this paper will be scaled to the melting temperature, $T = T^*/T_m^*$, where $T_m^* = 0.655$ [28], and T^* is the scaled temperature defined in paper I. For simulations with $T = 0.0015$, 8192 time steps were used with integration step size $h = 0.005$ which gives a frequency resolution of $\Delta\omega_{res} = 0.1534\omega$. For the higher temperature simulations, 4096 time steps were used with $h = 0.005$ for $T = 0.02$–0.45, and $h = 0.0035$ for $T = 0.45$–0.63, which give frequency resolutions of $\Delta\omega_{res} = 0.3068\omega$ and $\Delta\omega_{res} = 0.4383\omega$, respectively. Reducing the time step from $h = 0.005$ to $h = 0.0035$ at $T = 0.45$ does not alter the spectral density shape or linewidth. Details of how the Q-resolved phonon spectral densities were calculated during the MD simulations can be found in paper I. In some of the high-temperature ($T = 0.45$–0.63) simulations 30 to 40 runs were added together to resolve phonon lineshape features. These runs were taken consecutively, with the final coordinates from the preceding run providing the initial coordinates for the next run. For each temperature (except $T < 0.10$) at least two initial starting conditions were equilibrated for 5000 time steps for $T = 0.02$–0.10, and 10000 time steps for $T = 0.10$–0.63. Upon completion of the simulation, the atomic positions were checked to make sure that they had not moved out of their assigned lattice positions.

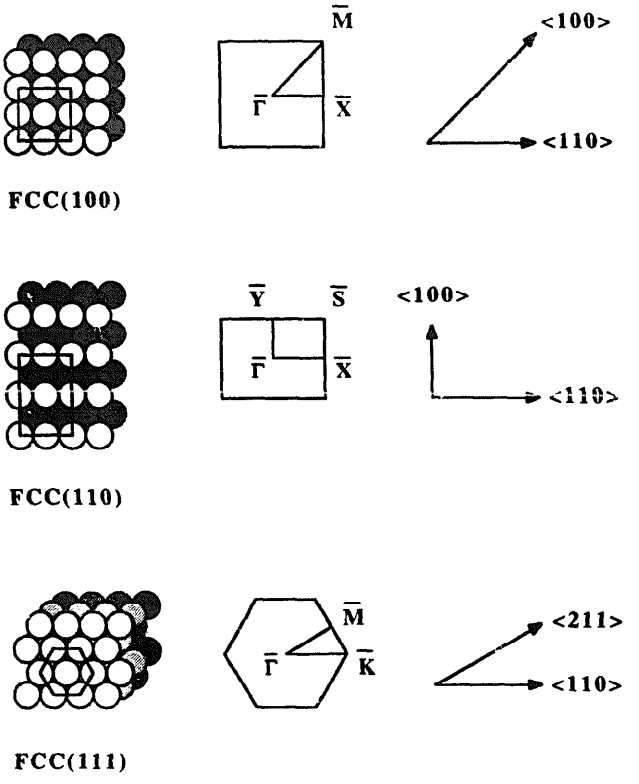

Fig. 1. Plotted in the left hand column of this figure are the geometric arrangement of atoms for fcc (100), (110), and (111) surfaces. In the middle column, are plotted the reciprocal lattice or surface Brillouin zone corresponding to each direct lattice. On the right-hand side are plotted the major directions in the surface plane. Note the ⟨110⟩ direction is always chosen in the nearest-neighbor direction.

3. Simulation results

The changes in the surface phonon spectra and the mean-square displacements were monitored as a function of increasing temperature. The phonon linewidths should have delta-function widths near $T = 0.0$ since, in the harmonic approximation, there is no mechanism for broadening. The z-polarized Rayleigh wave at $T = 0.0015$ is shown in fig. 2 for all three surfaces: the S_4 mode at $\bar{X}$ on the (100) surface, the S_1 mode at $\bar{X}$ on the (110) surface, and the S_1 mode near $\bar{K}$ on the (111) surface. Because of the way the 2D Fourier transform of the velocity vectors is calculated, the S_1 mode at $\bar{K}$ on the (111) surface is not sampled, but the S_1 mode at 90% of the surface Brillouin zone (SBZ) is sampled. This S_1 mode along the $\bar{\Gamma}$–$\bar{K}$ direction is the closest Q-vector to $\bar{X}$, and will be denoted as $\bar{K}^*$. These points of the SBZ were chosen since they correspond to vibrations between nearest- neighbor atoms. In fig. 2 the open circles are the MD calculated spectral density functions and the solid line is a fit to the MD data. The peaks were fit with a scaled Lorentzian function using a nonlinear least-squares fitting routine. These low-temperature simulations were run to make sure that the phonon widths were not artificially broadened by the periodic boundary conditions, or by integrator-induced round-off error. All three spectra have FWHM at the resolution of the simulation, and are essentially delta-functions at this low temperature. The frequency of each spectral density feature shown in fig. 2 agrees well with the frequency obtained using the slab technique as shown in paper I.

The effect of increased temperature on the line shapes of these phonons is shown in fig. 3. Three representative spectra for each surface are shown. For the (111) surface, temperatures up to $T = 0.611$ were simulated, while on the (110) surface only temperatures up to $T = 0.458$ were simulated (above this temperature the (110) surface starts disordering). A total of 35 simulation runs were used to calculate $T = 0.458$ on the (110) surface; a total of 40 runs were used to calculate the (111) surface at $T = 0.611$, and a total of 30 runs were used to calculate the (100) surface at

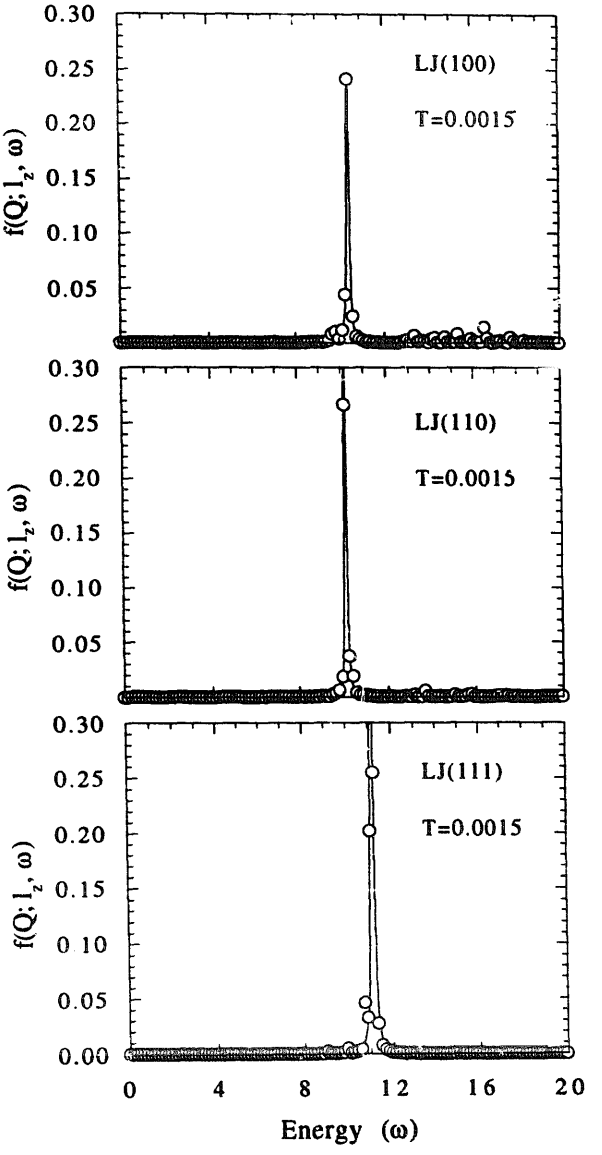

Fig. 2. Plot of the low-temperature (Rayleigh wave) phonon modes at $\bar{X}$ for the (100) surface, $\bar{X}$ for the (110) surface, and $\bar{K}^*$ (see text) for the (111) surface. These reciprocal space points correspond in direct space to nearest-neighbor vibrations.

$T = 0.534$. Each of the solid lines in fig. 3 were calculated using a nonlinear least-squares fitting program, where the surface phonon features were fit with Lorentzian functions and the background to the right of the phonon peak was fit by a Gaussian function. This Gaussian background is due to multiphonon and bulk phonon contributions to the surface spectral density, as observed in HAS and HREELS experiments [29,30].

The temperature dependencies of the frequencies for the modes plotted in fig. 3 are shown in fig. 4. The solid dots are the frequencies obtained from the Lorentzian fits to the spectral densities. The frequencies of all three modes decrease linearly with temperature. This decrease is primarily caused by the increase in lattice spacing which occurs as T is increased, i.e., from thermal expansion. The decrease in frequency can also be partially attributed to anharmonic effects at elevated temperatures.

The temperature dependencies of the frequencies shown in fig. 4 were least-squares fitted to $\omega = \omega_0 - \omega_1 T$, where ω is the frequency of the mode, ω_0 is the frequency at $T = 0.0$, and ω_1 is the slope. We have tabulated the slopes and intercepts from these fits in table 1. In this table the phonon modes are grouped according to their velocity component; $\hat{x}$, $\hat{y}$, or $\hat{z}$. The first column of the table shows the surface for each mode. In the second column of table 1 the surface mode assignment as derived by Allen, Alldredge and de

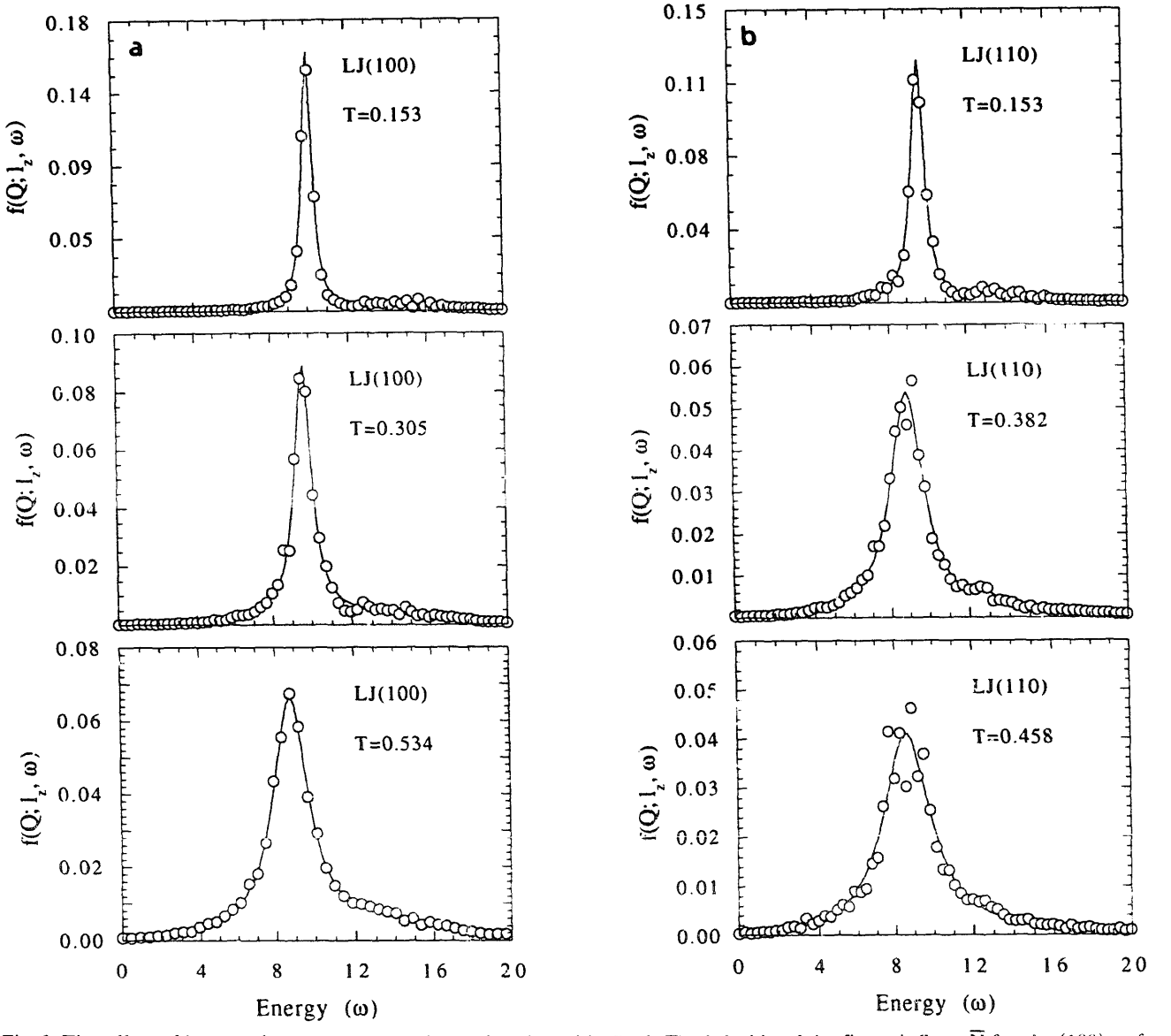

Fig. 3. The effect of increased temperature on the modes plotted in fig. 2. The left side of the figure is S_4 at $\bar{X}$ for the (100) surface, S_1 at $\bar{X}$ for the (110) surface, and S_1 at $\bar{K}$ (see text) for the (111) surface.

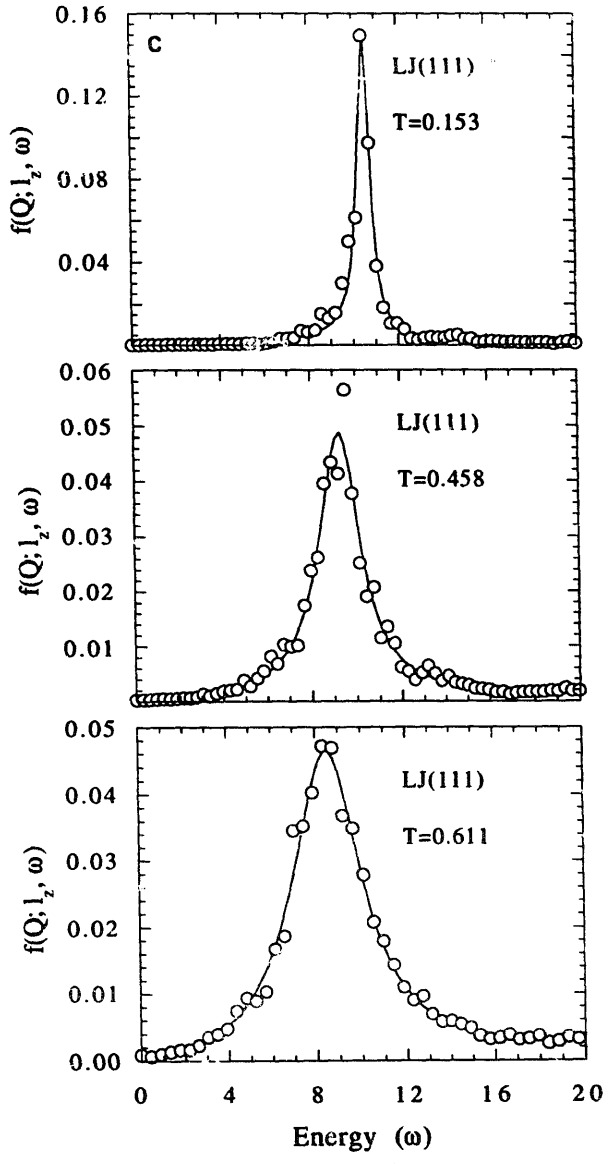

Fig. 3. Continued.

Wette is shown (these same assignments are used in fig. 2 of paper I). The third column of table 1 shows the high-symmetry reciprocal lattice points for each of the modes. In the fourth column, the $T = 0.0$ frequencies, ω_0, are shown, in the fifth column the slopes, ω_1, are shown, and in the last column the scaled slopes, ω_1/ω_0, are shown. We scale the slopes in this way so that the slopes of different modes can be directly compared to each other independent of the $T = 0.0$ frequency (which varied from $25.52–6.80\omega$). The scaled slopes for the three modes in fig. 4 are nearly identical, which is expected since these vibrations are the Rayleigh waves for these surfaces, all propagating along the ⟨110⟩ direction.

In an attempt to explain this decrease in frequency as the temperature is increased, slab technique (ST) calculations for the modes in fig. 4 were calculated as a function of temperature (the lattice spacing is changed to account for thermal expansion) and revealed scaled slopes equal to $\omega_1/\omega_0 = 0.25 \pm 0.01$ for all three surface modes. These scaled slopes calculated using the ST are about 17–30% less than the MD calculated scaled slopes shown in table 1. This discrepancy between the two methods occurs because all higher-order potential terms are included in the MD method, whereas only the first and second derivatives of the pair-potential are used in the ST calculation. Similar disagreement has also been observed in the MD simulations and ST calculations on Cu(110) [14].

Because the decrease (ω_1/ω_0) in frequency occurs both from thermal expansion of the lattice and anharmonic terms, an attempt was made to quantify the relative contribution of each. The anharmonic contribution to the frequency decrease will most likely be stronger for modes that are localized to the surface, since these vibrations will be more strongly effected by the temperature induced increase in atomic displacements. This measure was obtained using the eigenvector displacements, $|e^{\alpha}(Q; l_z)|^2$, which for vibrations

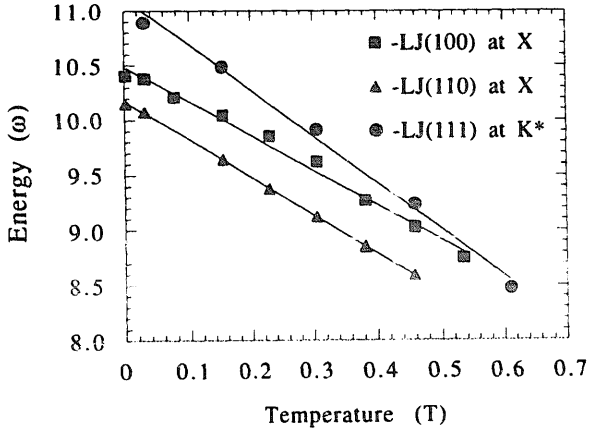

Fig. 4. Plot of the frequency decrease for modes in fig. 3 as a function of increasing temperature. The intercepts, slopes, and scaled slopes for these modes are shown in table 1.

Table 1
This table contains the linear fitting parameters of the phonon frequency as a function of temperature, T

Surface	Mode	Q	Intercept $\omega_0(\omega)$	Slope $\omega_1(\omega)$	Scaled slope ω_1/ω_0	Localization to surface
$\hat{x}$ component modes						
100	S_6	$\bar{X}$	22.30	5.74	0.253	0.10
110	S_7	$\bar{X}$	22.72	6.38	0.281	0.38
110	S_2	$\bar{Y}$	8.67	3.15	0.363	0.87
111	S_4	$\bar{M}$	25.52	5.00	0.196	0.15
$\hat{y}$ component modes						
100	S_1	$\bar{X}$	6.96	4.52	0.649	1.49
110	S_2	$\bar{X}$	12.34	4.87	0.395	0.06
110	S_1	$\bar{S}$	10.20	4.89	0.479	0.27
110	S_1	$\bar{Y}$	6.80	3.36	0.494	0.37
$\hat{z}$ component modes						
100	S_4	$\bar{X}$	10.51	3.15	0.300	0.23
100	S_1	$\bar{M}$	11.59	4.16	0.359	0.96
110	S_1	$\bar{X}$	10.17	3.63	0.357	0.16
110	S_2	$\bar{S}$	10.61	3.76	0.354	0.13
110	S_3	$\bar{Y}$	9.36	4.29	0.459	0.36
111	S_1	$\bar{M}$	10.52	3.41	0.324	0.23
111	S_1	$\bar{K}^*$	11.13	4.35	0.391	0.53

The modes are grouped according to their velocity component; $\hat{x}$, $\hat{y}$ or $\hat{z}$. The first three columns show the surface, the mode assignment given in ref. [48], and the Q vector where the mode was sampled. The fourth and fifth column give the intercept and negative slope of the linear fit to the temperature dependence data. The sixth column shows the scaled slope, ω_1/ω_0. The seventh column contains the mode's degree of localization to the surface, i.e., the larger the value the more localized the mode is to the surface. Its derivation is explained in the text.

localized to the surface decays exponentially into the bulk, i.e., increasing l_z. The rate of this decay or $\Delta(\log|e^{\alpha}(Q; l_z)|^2)/\Delta l_z$ is shown in table 1. The larger this decay the more localized this mode is to the surface. On the (100) and (111) surfaces, modes which have a large scaled slope tend to have a large localization to the surface. This correlation between scaled slope and localization to the surface is less true for the modes on the (110) surface in part because the scaled slopes, which on average are the largest, are more likely influence by anharmonic terms than modes on the (100) or (111) surfaces. The scaled slopes also tend to be larger on the (110) surface than the (100) or (111). The larger decrease of the S_1 mode on the (100) surface is most likely at-

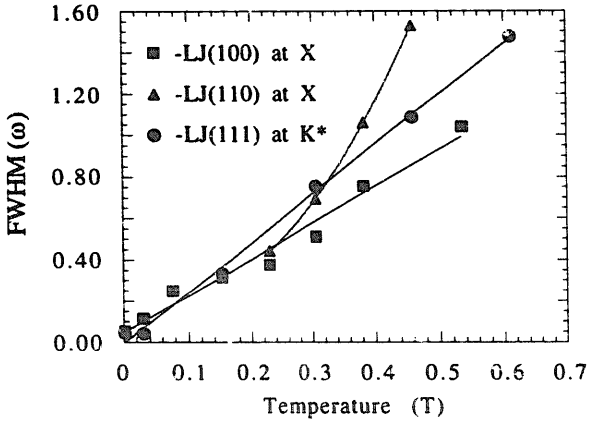

Fig. 5. Plot of the phonon width increase for the modes in fig. 3 as a function of increasing temperature. The phonon width's slope for the linear region for all three modes are shown in table 2. The quadratic fit for the (110) surface is also shown in table 2.

tributed to the increased localization to the surface ($\Delta(\log|e^{\alpha}(Q; l_z)|^2)/\Delta l_z - 1.49$).

The temperature dependencies of the linewidths shown in fig. 4 are plotted in fig. 5. Since the Rayleigh wave frequencies shown in fig. 4 are roughly the same, the widths plotted in fig. 5 were not scaled by the zero temperature frequency, ω_0, for each mode. In fig. 5, a straight line of slope W_1 was fit to the Rayleigh wave FWHM on the (111) and (100) surfaces, and on the (110) at low temperature. The intercepts here are zero, since the linewidths should be zero at $T = 0$. This linear dependence of the linewidths with increasing T worked well for S_4 on the (100) surface and S_1 on the (111) surface. *However, this linear trend does not fit the temperature dependence of S_1 on the (110) surface at temperatures greater than $T = 0.25$.* At these temperatures, this mode is better fit by a quadratic function given by $W(T) = W_0 + W_2(T - T_{AN})^2$, where W denotes the width of the mode, W_0 is the minimum in width of the parabola at T_{AN}, W_2 is the curvature of the parabola, and T_{AN} is the temperature where the width changes from a linear to a quadratic dependence on T. The fitted values for both the linear (column 4) and quadratic (column 5–7) fits (if needed) are shown in table 2, where the width coefficients have been scaled by the frequency, ω_0 (from column 4, table 1).

The linear increase in FWHM is due to single-phonon virtual exchange including dephasing), which Armand et al. have shown dominate phonon lifetimes at low temperature [16,17,31]. As the temperature is increased above $T = 0.25$, the FWHM for the S_1 mode on the (110) surface increases rapidly and deviates significantly from linear behavior. This deviation from a linear to a quadratic temperature dependence

Table 2
This table contains the linear and quadratic fitting parameters of the phonon linewidth as a function of temperature, T

Surface	Mode	Q	Linear $W(T) = W_0 T$ W_1/ω_0	Quadratic $W(T) = W_0 + W_2(T - T_{AN})$		
				W_0/ω_0	W_2/ω_0	T_{AN}
$\hat{x}$ component modes						
100	S_6	$\bar{X}$	0.115	0.035	3.75	0.30
110	S_7	$\bar{X}$	0.068	0.011	0.57	0.10
110	S_2	$\bar{Y}$	0.152			
111	S_4	$\bar{M}$	0.145	0.027	0.46	0.35
$\hat{y}$ component modes						
100	S_1	$\bar{X}$	0.169			
110	S_2	$\bar{X}$	0.135	0.031	1.05	0.17
110	S_1	$\bar{S}$	0.331			
L10	S_1	$\bar{Y}$	0.131	0.033	0.66	0.15
$\hat{z}$ component modes						
100	S_4	$\bar{X}$	0.188			
100	S_1	$\bar{M}$	0.229			
110	S_1	$\bar{X}$	0.194	0.036	1.18	0.15
110	S_2	$\bar{S}$	0.205			
110	S_3	$\bar{Y}$	0.219			
111	S_1	$\bar{M}$	0.223			
111	S_1	$\bar{K}^*$	0.216			

The first three columns are the same as in table 1. The fourth column gives the slope for the linear fit, W_1, and is scaled by the $T = 0$ frequency, ω_0 (column 4, table 1). The fifth through seventh columns have the fitting parameters for the modes that have a T^2 temperature dependence. Both W_0 and W_2 are scaled by ω_0.

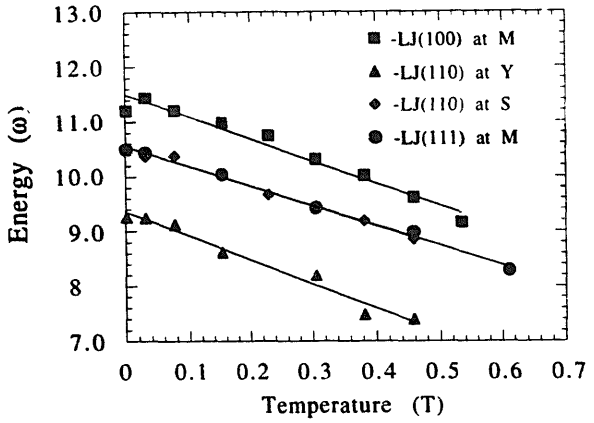

Fig. 6. Plot of the frequency decrease as a function of increasing temperature for Rayleigh modes at various high-symmetry points.

is due to increased contribution from phonon – phonon virtual exchanges [16,31]. These higher-order virtual-phonon exchanges begin to occur on the (110) surface at lower temperatures than on the (100) and (111) surfaces because of the larger thermally activated displacements which occur perpendicularly to the direction in which this mode propagates. The temperature at which the T^2 dependence begins to "turn-on" for S_1 at $\bar{X}$ on the (110) surface is $T_{AN} = 0.15$. We will present more on how the RMSD change with increasing temperature later in this paper.

The frequency dependencies of four other $\hat{z}$-polarized modes are plotted in fig. 6: S_1 at $\bar{M}$ on the (100) surface, S_2 at $\bar{S}$ on the (110) surface, S_3 at $\bar{Y}$ on the (110) surface, and S_1 at $\bar{M}$ on the (111) surface. The intercepts, slopes, and scaled slopes for these modes are tabulated in table 1. The temperature dependence of these modes have roughly the same slope as as the modes in fig. 4. The temperature dependence of these modes' FWHM are not plotted, but the temperature dependence of these modes' linewidths are shown in table 2.

This change in the phonon width from T to T^2 dependence also occurs on the (100) and (111) surfaces, but at significantly higher temperatures than on the (110) surface. T^2 dependent width changes were also observed in the $\hat{x}$ and $\hat{y}$ component spectra as shown in table 2. Two modes that with an $\hat{x}$ component of motion were found to have a T^2 temperature dependence. These modes are the S_6 at $\bar{X}$ on the (100) surface and the S_4 at $\bar{M}$ on the (111) surface. Both of these modes involve shear vertical motion and propagate perpendicular (S_4) or nearly perpendicular (S_6) to the direction of largest RMSD. Three additional modes were found on the (110) surface that displayed T^2 temperature dependence. These are the S_2 and S_7 at $\bar{X}$, and the S_1 at $\bar{Y}$. In fact, all three major modes, S_1, S_2 and S_7 at $\bar{X}$ on the (110) surface change to a T^2 temperature dependence. Each of the modes that display T^2 temperature dependence propagates perpendicular or nearly perpendicular to a direction of maximum RMSD, except the S_1 at $\bar{Y}$. (This mode is only weakly quadratic in temperature.) The temperatures at which the mode's FWHM changes from T to T^2 dependence is $T_{AN} = 0.30$ for the (100) surface, $T_{AN} = 0.15$ for the (110) surface and $T_{AN} = 0.35$ for the (111) surface.

Because the amount of the anharmonic potential the surface atoms sample depends on how far apart they move from each other, the root-mean-square displacements were also monitored during the simulation. The directional components of the RMSD for all three surfaces are plotted in fig. 7. *On the (110) surface near $T = 0.15$, the RMSD ($\hat{y}$-component) perpendicular to the rows become larger than the surface normal RMSD $\hat{z}$-component).* This is not surprising, since along this direction the nearest-neighbor distance is $\sqrt{2}$ larger than in the $\hat{x}$-direction. Experimental measurements of the MSD on Ni(110) indicate that the MSD perpendicular to the rows are larger than the MSD parallel to the rows [32]. Clark et al., using a simple force constant model, have found that the MSD perpendicular to the rows are 33% larger than the MSD parallel to the rows [33]. This larger RMSD perpendicular to the rows interferes with propagation of the S_1 mode along the row. When the RMSD perpendicular to the rows become larger than those normal to the surface, the probability for this mode to scatter into other modes increases. For comparison, the S_3 mode at $\bar{Y}$, which propagates perpendicular to the atom rows, does not show T^2 dependence, because the RMSD parallel to the rows are

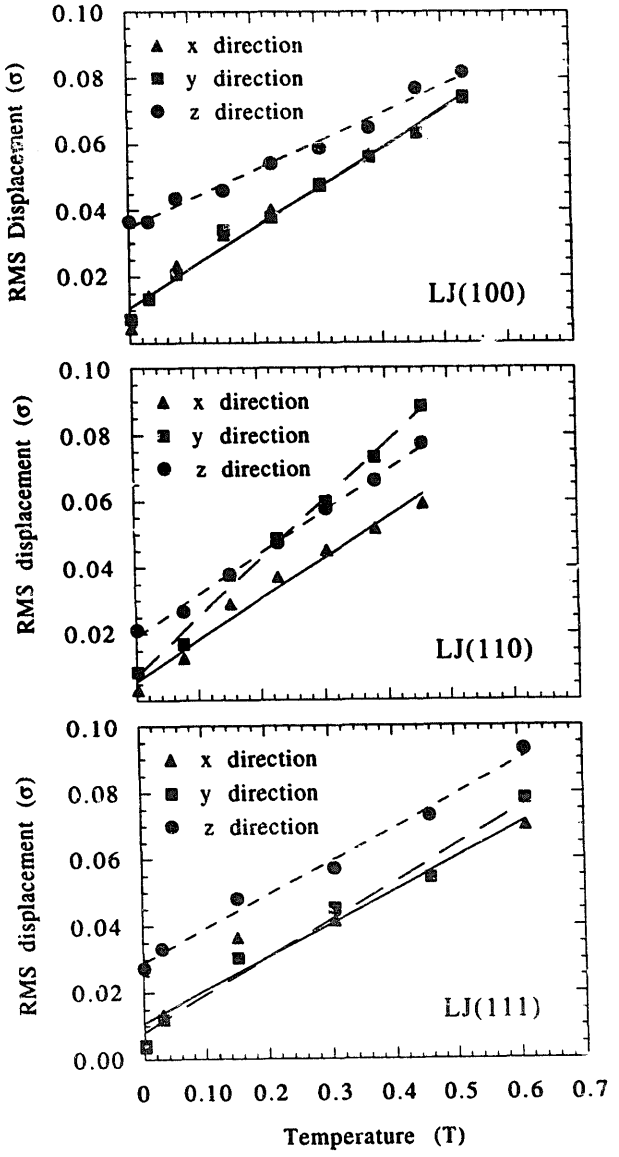

Fig. 7. Plot of the directional components RMSD for the (100), the (110), and the (111) surfaces. The x-component RMSD are represented by triangles, the y-component RMSD are represented by squares, and the z-component RMSD are represented by circles.

smaller than both the RMSD normal to the surface and perpendicular to the rows.

For work discussed up to this point, we have simulated surfaces where all atoms have maintained registry with the initial simulation positions; i.e., no diffusion events have occurred. At this point, we will discuss simulations were we have monitored the surface stress as a function of increasing temperature for an ordered (110) surface and a slightly disordered (110) surface. We perform this comparison to better understand the difference between the temperature induced structural changes and the temperature induced anharmonic changes in the RMSD and surface stress.

The disordering mechanism we observed, called an adatom–vacancy pair defect, is shown in fig. 8. It is created when one surface atom is promoted to the next surface layer, while the atom originally next to it in the lattice shifts in the $\hat{x}$-direction to take the adatoms' original position. Several authors have proposed that the creation of this defect is a possible initial disordering stage for surface melting and roughening [14,15,34]. Previously, de Lorenzi et al. estimated for two surface temperatures the frequency of adatoms single jumps were larger perpendicular to the atom rows on the (110) surface than along the atom rows [35]. These authors indicate that the adatoms which are promoted to ontop of the surface remain relatively fixed until the next diffusion event [35].

In our simulations, we witnessed the creation of one of these adatom–vacancy pair defects for a simulation size of $12 \times 12 \times 41$ at $T = 0.458$. The defect appeared during the simulation near the 58000th integration time step and no further defect pairs were observed up to the completion of the simulation at the 123000th time step. For a slightly smaller sized simulation $10 \times 10 \times 31$ at $T = 0.458$, no defect pairs were observed up to

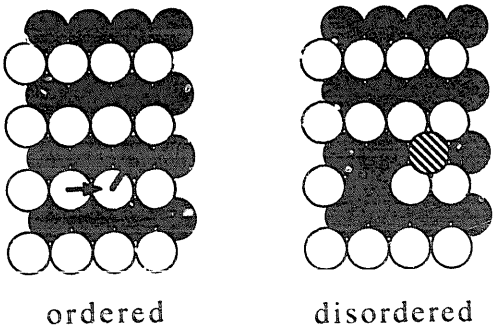

Fig. 8. Plot of the adatom–vacancy defect-pairs creation mechanism observed on the (110) surface. The left-hand side shows the directions that the atoms are displaced and the right hand side shows the final arrangement of atoms. The striped circle denotes the adatom and the black circle denotes the vacancy.

Table 3
This table contains the first- and second-layer RMSD for the ordered and disordered surface depicted in fig. 8 (the simulation temperature was $T = 0.453$)

Layer	Type	Mean-square displacements ($\times 10^{-2}\sigma$)			
		$\hat{x}$	$\hat{y}$	$\hat{z}$	Total
1 st	Ordered	5.93	8.82	7.74	13.14
	Disordered	6.13	9 07	7.87	13.49
2 nd	Ordered	4.82	5.39	5.95	9.37
	Disordered	4.80	5.48	6.02	9.44

the 123 000th time step. This indicates that the creation of one of these defects is a rare event. However, this cannot rule out the possibility that the periodic boundary conditions or different sizes of the simulations might also be playing a significant role.

Because the creation of this defect is rare at this temperature, it was not studied in detail but a surface that contains one defect pair or was simulated. In table 3 we show the changes in the first- and second-layer RMSD (all three directional components) for an ordered (110) surface and a "disordered" (110) surface that contains one adatom–vacancy pair defect. All RMSD values for the "disordered" (110) surface are slightly larger than RMSD for the ordered surface, except for the $\hat{x}$-component in the second layer. When *averaged* over the 100 surface atoms, the first-layer surface normal RMSD are 2.6% larger on the disordered surface than on the ordered surface. This implies that the increase in the RMSD on the disordered surface is small compared to the relative increase in the RMSD from the anharmonic potential terms. Over the entire integration time the $12 \times 12 \times 41$ dimensioned (110) surface was simulated, we estimate that the creation of only one adatom–vacancy defect pair is possible. If the creation of additional defect pairs were possible, we believe that the creation of additional defects should occur fairly rapidly after the creation of the initial defect. However, no additional defects were observed between the 58 000th and 123 000th time step.

Even though the increase in the RMSD for the creation of one adatom–vacancy pair defect is small compared to the anharmonic contribution, the creation of just one of these defects relieves a substantial amount of in-plane surface stress. Previous studies of the calculated surface stress on the (110) surface show that a positive tensile stress exists along the rows ($\hat{x}$-direction) and a negative compressive stress exists perpendicularly

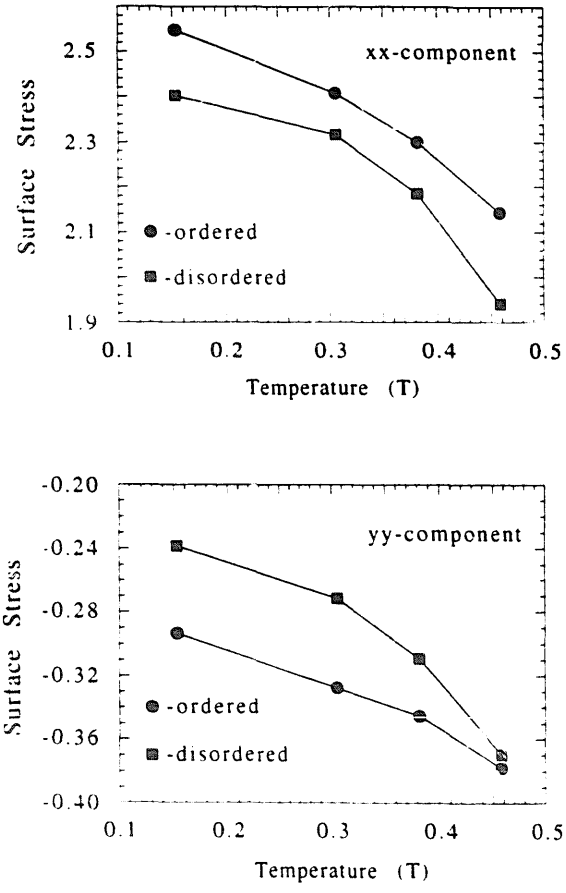

Fig. 9. Plot of the xx and yy tensor components of the surface stress as a function of temperature for the two configurations shown in fig. 8.

to the rows ($\hat{y}$ -direction) [23]. At temperatures corresponding to $T = 0.25$, the surface stress components begin to decrease towards zero [23]. Surface stress arises because of the reduction in the number of nearest neighbors at the surface. As explained in paper I, the minimum in the potential energy for a two-dimensional sheet of atoms occurs at a slightly larger lattice spacing than the bulk lattice spacing. Because the surface atoms sit in registry with the bulk lattice spacing, they do not sit at their intraplanar potential minimum, and the first derivative of the total surface potential energy at the surface is nonzero. Normal to the surface plane, this stress is relieved through expansion of the interlayer spacing. However in the surface plane the atoms are held laterally fixed to their bulk-terminated positions and no net relaxation takes place.

A plot of the *xx* and *yy* tensor components of the surface stress at four different temperatures for the ordered (110) surface and a (110) surface with one adatom–vacancy defect pair is plotted in fig. 9. We find at $T = 0.153$ that the *xx*-component of the stress is reduced by 5.8% and the *yy*-component of stress is reduced by 18.8%. The stress components decrease as the temperature is increased and at $T = 0.453$ the *yy*-component for the ordered and disordered surface become almost equal, while the *xx*-component on the disordered surface is 9.4% lower than on the ordered surface. Our results agree qualitatively with the results of Broughton and Gilmer who observed a reduction in the magnitude of the surface stress as the number of surface defects increased [23].

4. Discussion

In this paper we reported the results of temperature dependent MD simulations of the surface phonon spectral densities and RMSD for fcc (100), (110), and (111) surfaces. These results were obtained using a LJ pair potential to describe the interactions and to calculate how the anharmonic potential terms effect the surface lattice dynamics. While our results obtained using LJ potentials are a good starting for understanding how anharmonic potential terms influence surface vibrations, our results do not necessarily apply to real materials, such as metals and semiconductors, because they are too anharmonic. We are currently calculating the surface phonon spectral densities using the Finnis–Sinclair (FS) model (Sutton potentials) suitable for Ni(110) and Cu(110) surfaces. When this papers results are compared with the FS model results it will better illuminate the difference between pair potentials and many-body potentials especially how the anharmonic potential terms from the two different models influence the surface lattice dynamics.

The MD simulations performed by Ditlevsen et al. using EMT based potentials on Cu(110) [14] have recently been compared to the HREELS data taken by Baddorf and Plummer [10,11]. These simulations reproduce the experimentally observed slopes for both the decrease in frequency ($\omega_1/\omega_0 = 0.21$) and the linear increase in width ($W_1/\omega_0 = 0.32$) for the S_3 mode at $\bar{Y}$. However, the absolute value of the frequencies and widths do not match. Our results in table 2 show that this mode's width will have a linear dependence on temperature up to half its melting temperature, which is remarkably similar to the HREELS data [10,11]. Our predicted decrease in frequency is twice as much as the experimental data, however our predicted increase in width is about $\frac{2}{3}$ less than for the EMT results. This implies that this surface mode on Cu is more strongly influenced by the anharmonic terms than what we observed on the (110) LJ surface. This might be expected, since the surface atoms bound by LJ potentials are always relaxed outward from the surface plane in contrast to surface atoms on noble metals which are displaced inward toward the second layer [36–40]. Perhaps this inward relaxation in conjunction with the increased MSD allow the surface atoms to experience more of the anharmonic part of the potential, than for LJ potentials.

Subtle differences are observed between the temperature dependence of the RMSD in our simulations and the temperature-dependent simulations performed for Ni(100), Ni(110), and Ni(111) calculated using the embedded-atom method [15,41]. Unlike our simulations where the surface normal RMSD always increase continu-

ously from the bulk to the surface, the Ni(110) first layer RMSD normal to the surface are lower then the second-layer RMSD normal to the surface [15]. This effect is due to the increase in the embedding potential as a consequence of the decreased atomic surface density [42]. However, the RMSD normal to the atomic rows on the Ni(110) surface are larger than the RMSD along the atomic rows or normal to the surface plane [15], which is in agreement with our simulation results. This implies that at $\bar{X}$ on Ni(110) the surface phonon modes might display a T to T^2 change in linewidth as the temperature of the surface is heated.

5. Conclusions

We have reported how increased temperature effects the surface phonon spectral densities of LJ solids. We find that as the temperature is increased, the frequency of all modes decrease linearly in temperature, while the modes' widths increase linearly at low temperature, and for some modes quadratically at higher temperatures. The temperature at which the transition from linear to quadratic T dependence dominates the linewidth depends on the surface face. These temperatures are approximately $T_{AN} = 0.30$ for the (100) surface, $T_{AN} = 0.15$ for the (110) surface, and $T_{AN} = 0.35$ for the (111) surface. The linear temperature dependence of the linewidth is believed to be dominated by single phonon–phonon scattering while the quadratic dependence is due to the increase of a single phonon into higher-order phonon scattering events [16,17]. Also, the linear to quadratic temperature dependence change of the linewidth occurs for modes which propagate normal or nearly normal to the direction of maximum RMSD.

The change from linear to quadratic width dependence occurs on the (110) surface at a lower temperature ($T_{AN} = 0.15$) than the (100) and (111) surfaces. Near this temperature the RMSD perpendicular to the rows on the (110) surface become larger than the RMSD normal to the surface plane at $T = 0.15$. Because of the increased RMSD perpendicular to the rows, the Rayleigh wave's width at $\bar{X}$ changes from a linear to a quadratic temperature dependence, as seen in fig. 5. Our results support claims [9] that increases in measured RMSD for some systems can be due to increased surface anharmonicity rather than from surface roughening. In a forthcoming paper we will examine whether similar temperature dependent changes occur for Ni(110) and Cu(110) using a Finnis–Sinclair potential model [43,44].

Although the initial decrease in the RMSD is due to the anharmonic potential terms, small amounts of surface disorder will further increase the RMSD. We have shown that the amount of RMSD increase for a "disordered" surface that has one adatom–vacancy defect pair is small compared to the anharmonic contribution [14,15,34]. The RMSD on the "disordered" surface which contains one adatom defect pair are only 2.6% larger when averaged over 100 surface atoms than the RMSD for an ordered surface. However the creation of this defect on the (110) surface relieves a substantial amount of in-plane surface stress. The creation of this defect pair reduces the xx-component of the stress by 5.8% and the yy-component of stress is reduced by 18.8% when compared to the ordered 100 atom surface at the same temperature. Stress reduction as a consequence of this defect creation may be important for a more thorough understanding of temperature driven phenomena at surfaces such as melting, the initial stages of epitaxial growth, and reductions in chemisorption energies upon adsorption due to geometric relaxation of the surface [15,45–47].

Acknowledgements

We wish to acknowledge many helpful conversations with P.A. Knipp. We also thank D.L. Mills, D.F. Padowitz, L. Brown, S.F. King and T. Curtiss. This work was supported, in part, by the Air Force Office of Scientific Research and the National Science Foundation Materials Research Laboratory at The University of Chicago.

References

[1] G.A. Held, J.L. Jordan-Sweet, P.M. Horn, A Mak and R.J. Birgeneau, Phys. Rev. Lett. 59 (1987) 2075.
[2] S.G.J. Mochrie, Phys. Rev. Lett. 59 (1987) 304.
[3] B. Salanon, F. Fabre, D. Gorse and J. Lapujoulade, J. Vac. Sci. Technol. A 6 (1988) 655.
[4] J. Lapujoulade, Surf. Sci. 178 (1986) 406.
[5] U. Breuer, O. Knauff and H.P. Bonzel, Phys. Rev. B 41 (1990) 10848.
[6] J.W.M. Frenken, R.J. Hamers and J.E. Demuth, J. Vac. Sci. Technol. A 8 (1990) 293.
[7] H. Yang, T. Lu and G. Wang, Phys. Rev. B 43 (1991) 4714.
[8] Y. Cao and E.H. Conrad, Phys. Rev. Lett. 64 (1990) 447.
[9] P. Zeppenfeld, K. Kern, R. David and G. Comsa, Phys. Rev. Lett. 62 (1989) 63.
[10] A.P. Baddorf and E.W. Plummer, J. Electron Spec. Rel. Phenom. 54/55 (1990) 541.
[11] A.P. Baddorf and E.W. Plummer, Phys. Rev. Lett. 66 (1991) 2770.
[12] R. Franchy, M. Wuttig and H. Ibach, Surf. Sci. 203 (1988) 489.
[13] K. Kern, U. Becher, P. Zeppenfeld, G. Comsa, B. Hall and D.L. Mills, Chem. Phys. Lett. 167 (1990) 362.
[14] P.D. Ditlevsen, P. Stoltze and J.K. Nørskov, Phys. Rev. B (1991), submitted.
[15] E.T. Chen, R.N. Barnett and U. Landman, Phys. Rev. B 41 (1990) 439.
[16] G. Armand and P. Zeppenfeld, Phys. Rev. B 40 (1989) 5936.
[17] G. Armand, D. Gorse, J. Lapujoulade and J.R. Manson, Europhys. Lett. 3 (1987) 1113.
[18] D.D. Koleske and S.J. Sibener, J. Electron Spectrosc. Relat. Phenom. 54/55 (1990) 363.
[19] P. Knipp, Phys. Rev. B 43 (1991) 6908.
[20] D.D. Koleske and S.J. Sibener, Surf. Sci. 268 (1991) 406.
[21] M.R. Mruzik and G.M. Pound, J. Phys. F (Metal Phys.) 11 (1981) 1403.
[22] J.Q. Broughton and L.V. Woodcock, J. Phys. C (Solid State) 11 (1978) 2743.
[23] J.Q. Broughton and G.H. Gilmer, J. Chem. Phys. 79 (1983) 5105.
[24] J.Q. Broughton and G.H. Gilmer, J. Chem. Phys. 79 (1983) 5095.
[25] J.Q. Broughton and G.H. Gilmer, J. Chem. Phys. 79 (1983) 5119.
[26] R.E. Allen, F.W. de Wette and A. Rahman, Phys. Rev. 179 (1969) 887.
[27] A.R. McGurn, A.A. Maradudin, R.F. Wallis and A.J.C. Ladd, Phys. Rev. B 37 (1988) 3964.
[28] W. Schommers, in: Structure and Dynamics of Surfaces I, Eds. W. Schommers and P. von Blackenhagen (Springer, Berlin, 1986).
[29] K. Kern and G. Comsa, in: Molecule Surface Interactions, Ed. K.P. Lawley (Wiley-Interscience, Chichester, 1989).
[30] H. Ibach and D.L. Mills, Electron Energy Loss Spectroscopy and Surface Vibrations (Academic Press, New York, 1982).
[31] G. Armand, J.R. Manson and C.S. Jayanthi, Phys. Rev. B 34 (1986) 6627.
[32] A.U. MacRae and L.H. Germer, Phys. Rev. Lett. 8 (1962) 489.
[33] B.C. Clark, R. Herman and R.F. Wallis, Phys. Rev. 139 (1965) 860.
[34] V. Rosato, G. Ciccotti and V. Pontikis, Phys. Rev. B 33 (1986) 1860.
[35] G. de Lorenzi, G. Jacucci and V. Pontikis, Surf. Sci. 116 (1982) 391.
[36] S. Lehwald, J.M. Szeftel, H. Ibach, T.S. Rahman and D.L. Mills, Phys. Rev. Lett. 50 (1983) 518.
[37] S. Lehwald, F. Wolf, H. Ibach, B.M. Hall and D.L. Mills, Surf. Sci. 192 (1987) 131.
[38] W. Menezes, P. Knipp, G. Tisdale and S.J. Sibener, Phy. Rev. B 41 (1990) 5648.
[39] P.D. Ditlevsen and J.K. Nørskov, J. Electron Spectrosc. Relat. Phenom. 54/55 (1990) 237.
[40] J.S. Nelson, E.C. Sowa and M.S. Daw, Phys. Rev. Lett. 61 (1988) 1977.
[41] E.T. Chen, R.N. Barnett and U. Landman, Phys. Rev. B 40 (1989) 924.
[42] J.S. Nelson, M.S. Daw and E.C. Sowa, Phys. Rev. B 40 (1989) 1465.
[43] M.W. Finnis and J.E. Sinclair, Philos. Mag. A 50 (1984) 45.
[44] A.P. Sutton and J. Chen, Philos. Mag. Lett. 61 (1990) 139.
[45] P. Stoltze, J.K. Nørskov and U. Landman, Phys. Rev. Lett. 61 (1988) 440.
[46] P.J. Feibelman, J. Vac. Sci. Technol. A 8 (1990) 2548.
[47] P.J. Feibelman, Phys. Rev. Lett. 63 (1989) 2488.
[48] R.E. Allen, G.P. Alldredge and F.W. de Wette, Phys. Rev. B 4 (1971) 1661.